Etch mechanism of an Al_2O_3 hard mask in the Bosch process

Martin Drost [a,*], Steffen Marschmeyer [a], Mirko Fraschke [a], Oksana Fursenko [a], Florian Bärwolf [a], Ioan Costina [a], Mamathamba Kalishettyhalli Mahadevaiah [a], Marco Lisker [a,b]

[a] IHP GmbH – Innovations for High Performance Microelectronics, Im Technologiepark 25, 15236 Frankfurt (Oder), Germany
[b] Technische Hochschule Wildau, Hochschulring 1, 15745 Wildau, Germany

ARTICLE INFO

ABSTRACT

The etching of high aspect ratio structures in silicon via the Bosch process is essential in modern technologies such as microelectromechanical systems (MEMS) and through-silicon vias (TSV) fabrication. The process can be very demanding on the mask selectivity due to long etching times, and it has been shown that an Al_2O_3 hard mask is very suitable in this regard, as it offers significantly higher selectivity compared to the conventional SiO_2 or resist masks. In this work, we employ a combination of Scanning Electron Microscopy (SEM), Spectroscopic Ellipsometry (SE) and X-Ray Photoelectron Spectroscopy (XPS) depth profiling to scrutinize the Al_2O_3 mask etching mechanism and therefore the origin of the extraordinary high selectivity. We demonstrate that by increasing the passivation step time, a thicker fluorocarbon polymer layer is formed on the Al_2O_3, and Al_2O_3 is then removed with a minuscule average etch rate of $\sim$0.01 nm/min. XPS depth profiling reveals that during Deep Reactive Ion Etching (DRIE) using the Bosch process, an AlF_x layer is formed between the polymer and Al_2O_3. As AlF_x is non-volatile, it requires sputtering to be removed. If the polymer layer is thick enough to attenuate the incoming ions such that their energy is not sufficient to lead to desorption of AlF_x, such as when using a longer passivation time, the mask is not eroded. By investigating the surface after different amounts of DRIE cycles, we also obtained information about the formation rate of AlF_x and the changes in the Al_2O_3 and polymer thicknesses over the course of a DRIE process. These findings further expand the knowledge of DRIE and can help process engineers to tailor the processes accordingly.

1. Introduction

Deep Reactive Ion Etching (DRIE) is a fundamental process in technologies such as microelectromechanical systems (MEMS) [1] and through-silicon vias (TSV) for 3D-packaging [2,3]. For high aspect ratio etching of silicon, the time-multiplexed Bosch process is the typical process of choice for high volume manufacturing, as it is less demanding on the hardware compared to its main alternative, cryogenic DRIE. The Bosch process consists of a repeated sequence of sidewall passivation by fluorocarbon polymer deposition from C_4F_8, polymer removal at the bottom of the structure, and isotropic Si etch using SF_6. The alternation of passivation and isotropic etch leads to characteristic scallops at the sidewalls. Initially, the polymer removal and isotropic etch were done in a single step by applying a platen bias during the exposure to SF_6 plasma, and later developments separated these steps for improved process control [4]. The fabrication of high aspect ratio structures, such as in through-wafer etching, can be very demanding on the selectivity

towards the mask material due to long processing times, and a conventional SiO_2 hard mask may not provide this required selectivity. For this reason, the use of various metals (e.g. Al, Cr [5,6]), metal oxides (e. g. Al_2O_3, TiO_2, Cr_2O_3 [7–9]) and nitrides (e.g. AlN, ScAlN [10]) as mask materials in DRIE, including continuous processes, has been investigated. Out of these, Al_2O_3 has emerged as a very powerful candidate, as remarkable selectivities of up to 100,000:1 in a Bosch process have been reported [8]. Atomic Layer Deposition (ALD) allows the fabrication of high quality conformal layers, and structuring can be done with relative ease by various RIE chemistries and process conditions [8] [11,12]. Post DRIE the mask can be removed e.g. by H_3PO_4-based wet etch with high selectivity to Si and SiO_2 [13] (see also SI Fig. 1), which can also be used to pattern the Al_2O_3. The origin of the high selectivity in the Bosch process, however, is not yet understood in full detail. Due to the complexity of the process, a simple comparison of bond dissociation energies of different mask materials is not sufficient (compare e.g. ΔH (Al—O) = 512 ± 4 kJ/mol, ΔH(Si—O) = 798 ± 8 kJ/mol [14]). When

---

using feed gases that contain F, Al can form non-volatile reaction products in the form of AlF_3. These can be removed by sputtering, which is a source of micromasking due to redepositing of the non-volatile material [10]. However Al_2O_3 etch rates of <0.1 nm/min [8] suggest that sputtering is negligible under certain process conditions. In contrast, investigations with continuous inductively coupled plasma (ICP) etching have shown higher etch rates with F-based plasma compared to Cl- and Br-based ones [11]. Therefore, the objective of this work is to scrutinize the Al_2O_3 hard mask etch mechanism during DRIE and provide a clear explanation for the origin of the extraordinary high selectivity. A particular focus also lies on time-resolved measurements of possible chemical changes at the mask surface over the course of a DRIE process. To do so, we use a combination of Scanning Electron Microscopy (SEM), Spectroscopic Ellipsometry (SE) and X-Ray Photoelectron Spectroscopy (XPS) depth profiling.

2. Materials and methods

75 nm thick amorphous, stoichiometric Al_2O_3 layers were grown on 200 mm Si(100) wafers by thermal ALD using an ASM Pulsar process module. The layers were grown at 300 °C using the precursors $Al(CH_3)_3$ and H_2O. Al_2O_3 patterning was done with a resist mask, which was structured using a Nikon NSA SF-150 i-line tool. Al_2O_3 dry etching was done in an Applied Materials mxP capacitively coupled plasma (CCP) reactor, using Ar/BCl_3 gas chemistry with 80/50 sccm, 50 mTorr and 500 W platen power. Prior to this process, the chamber was conditioned using the same process with two blanket resist wafers. The remaining resist on Al_2O_3 was removed with oxygen plasma in the same chamber and a subsequent wet clean (ACT 935) step. DRIE experiments were performed in a Tegal 200 ICP reactor using a three step Bosch process. Prior to the DRIE processes, the chamber was conditioned using a blanket Si wafer, and subsequently a blanket wafer with 50 nm Al_2O_3, each for 10 min. The table temperature was 10 °C in all experiments. The source power frequency was 13.56 MHz and the pulsed bias power frequency was 270 kHz. SEM cross section images were recorded with a Zeiss Merlin Gemini 2 tool, with a beam energy of 1.5 keV. Minor adjustments to brightness and contrast were made to enhance visibility of important features. Thickness measurements with optical constant determination were performed by SE using a KLA Spectra Fx 200 tool. The wafers were measured after DRIE, without any further processing. After DRIE, the samples were transported at air to an XPS chamber outside the clean room. The measurements were performed in a Physical Electronics Instruments Versaprobe II instrument with a background

pressure $< 10^{-10}$ mbar, using an Al K_α X-ray source. Sputter depth profiles were recorded using an Ar ion source with $E_{kin,Ar} = 500$ eV, and sample charging was compensated using low energy Ar ions and electrons. The sputter time between the individual measurements was one minute. Quantification was done by dividing the integrated signals by the respective sensitivity factors, which were provided by the tool supplier software. The resulting depth profile curves were smoothed once with binomial smoothing. The individual spectra were fitted after a Shirley background subtraction.

3. Results and discussion

First, it was verified with SEM cross sections that the hard mask opening and DRIE processes lead to sufficiently good results when etching high aspect ratio structures. Fig. 1a) depicts the cross section of two annular TSV structures, with a ring width of 3 μm, and the inner region still standing intact (not cleaved). The DRIE etch recipe used is shown in Table 1. The process duration was 378 DRIE cycles ($\triangleq$ 60 min total etch time), with one cycle consisting of the sequence polymer passivation, polymer removal, and isotropic Si etch. The resulting TSV depth was ~230 μm. The quality of the structure geometry, in particular of the sidewalls, was found to be as good as with a conventional SiO_2 mask. Fig. 1b shows the edge of the mask and a TSV, directly after DRIE without further cleaning. The Al_2O_3 mask is almost intact, and is only thinned towards the etched structure. The thin fluorocarbon polymer film on top, which is known to form on the mask in DRIE, can be clearly identified.

However, we also observed micromasking in larger structures, i.e.

Table 1
Table of the most important parameters of the three step Bosch process recipe used in this work. The passivation step time in step 1 was varied in the experiments, as described in the text.

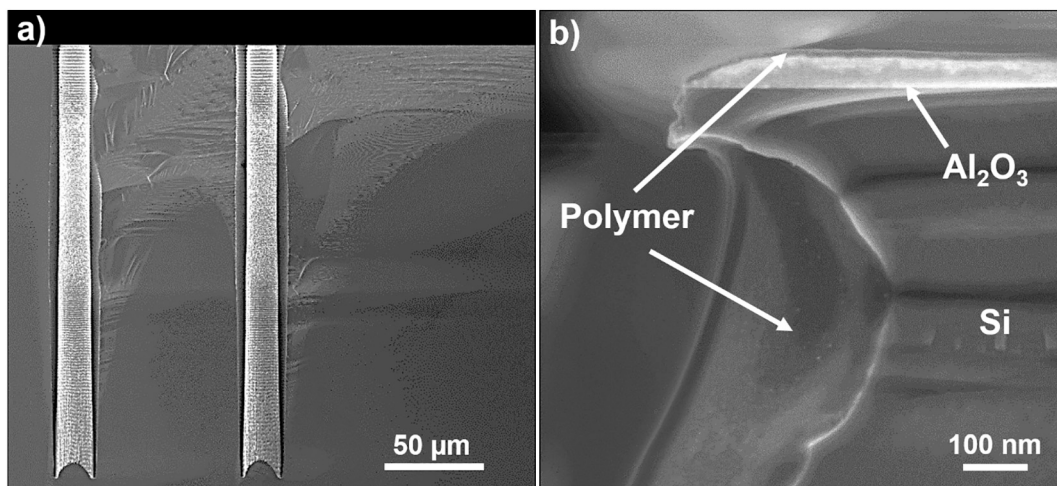|	Step 1	Step 2	Step 3
	Polymer passivation	Polymer removal	Isotropic Si etch
SF_6 flow / sccm	0	700	700
C_4F_8 flow / sccm	200	0	0
O_2 flow / sccm	15	0	0
Step time / s	varied: 2.2 / 4.0	1.5	4.5
P(Bias) / W	0	80 (pulsed)	0
t_{on} and t_{off} / ms	–	30 / 30	–
P(Source) / W	3000	2300	2300
p / mTorr	75	52	90

Fig. 1. a) SEM cross section of two annular TSV structures, fabricated with an Al_2O_3 hard mask and 378 cycles of the DRIE recipe shown in Table 1, with a passivation step time of 3.5 s; b) SEM cross section of the edge of the Al_2O_3 hard mask and an etched structure, after DRIE and without further cleaning, showing that a thin polymer layer forms on top of the mask, and that the mask becomes thinner towards the edge.

squares with >40 μm side length. As micromasking was not observed using the same etch recipe with a SiO_2 hard mask, we assume it is due to redepositing of mask material, possibly in the form of Al_2O_3 or AlF_x. The reason why formation of micromasking was not observed in smaller structures is presumably its aspect ratio dependence, which was recently demonstrated by Bagolini et al. for an Al hard mask [5]. Therein, the authors also show that micromasking can be avoided by a sacrificial layer on top of the mask, such as SiO_2 or photoresist. When this sacrificial layer is etched away, the aspect ratio is high enough such that no micromasking material is deposited at the bottom of the structure anymore.

Next, the thickness changes of the Al_2O_3 and the polymer on top as a function of the number of DRIE cycles were investigated. Again, the DRIE process given in Table 1 was employed. Fig. 2 depicts the thicknesses measured by SE, for two different passivation step times t_{pass} = 2.2 s and 4.0 s. Each data point corresponds to the mean value of four data points that were measured at the half radius of the wafer (one data point per wafer quadrant). The error bars depict the respective minimum and maximum values. The reason for the relative significant scatter of some data points is the strong correlation between the parameters in the 2-layer dielectric stack, consisting of thin polymer/Al_2O_3, on the Si substrate used for the modelling procedure by SE. The separation of two thicknesses can produce the small resulting thickness deviations due to optical constants deviation, especially with the presence of an ultra-thin interface layer (as shown below), which we observe as error bars in Fig. 2. Another important factor for the deviations can certainly be inhomogeneous processing in DRIE. We observe that after 360 cycles, for t_{pass} = 2.2 s the Al_2O_3 thickness decreases with an average etch rate of ~0.3 nm/min, whereas for t_{pass} = 4.0 s, the thickness decreases with an average etch rate of ~0.01 nm/min, i.e. it remains practically unchanged. For both passivation times, the polymer thickness increases to several nm within the first five cycles, and then appears to reach an approximate steady-state thickness, although there is significant scatter at some data points. Using t_{pass} = 4.0 s, the polymer is roughly twice as thick throughout the process with ~10–20 nm, compared to ~5–10 nm with t_{pass} = 2.2 s. We can therefore conclude that by increasing the passivation time, less Al_2O_3 is removed to the point where the selectivity is practically infinite.

Changes in chemical composition of the polymer/mask interface were monitored by XPS depth profiling measurements. Various samples were investigated after DRIE without further cleaning, i.e. with the polymer still on top. Fig. 3a depicts the atomic concentration of the four detected elements C, F, Al and O as a function of the sputter time, from a

sample processed for 180 cycles with t_{pass} = 4.0 s. Note that no S was detected despite the use of SF_6 in the polymer removal and isotropic etch steps. As expected, the relative C concentration decreases as the polymer is sputtered away after a brief increase in the top layers. The relative F concentration however increases between ~20–30 min sputter time, before it decreases again. As the polymer is removed the relative Al and O concentrations increase, however considerably more Al than O is detected until ~50 min sputter time, and only after that the stoichiometry of Al_2O_3 is attained. In Fig. 3c, selected spectra of the Al2p region at different sputter times are shown. The signals can be deconvoluted into two peaks separated by ~1.3 eV, which we attribute to Al_2O_3 (~75.8 eV) and an AlF_x compound (~77.1 eV) [15,16]. Initially at 20 min sputter time, the AlF_x peak dominates the spectrum, and with increasing sputter time the relative intensity of the Al_2O_3 peak increases and eventually is the only one remaining. In the F1s spectra, no such clear separation of peaks was observed, which might be because the signals from C_xF_y and AlF_x are not sufficiently separated to be resolved. The presence of the AlF_x peak coincides with the increased Al/O ratio. Therefore it can be concluded that the ratio Al/O > 1 in the first ~50 min sputter time and the relative increase in F concentration are due to the presence of an AlF_x layer at the interface between polymer and Al_2O_3.

In order to ensure that the fluorination of Al_2O_3 actually occurs during the DRIE process and is not an artifact induced by the depth profile sputtering, e.g. due to sputter induced defluorination of the polymer [17], a reference sample was investigated. This sample consisted of a polymer deposited on Al_2O_3 using only the polymer deposition step from Table 1 with t_{pass} = 4.0 s, resulting in a thickness of ~45 nm measured by SE. This reference sample allows attributing the change in composition to either being induced 1) by the depth profile sputtering when both samples exhibit it, or 2) by DRIE when only the fully processed sample exhibits it. Fig. 3b depicts the respective depth profile of the reference sample, with a longer sputter time due to the thicker polymer. Again, as the polymer is removed, the C and F concentrations decrease and the Al and O concentrations increase. However, in contrast to the sample processed by DRIE, there is no increase in relative F concentration, and the Al/O ratio mostly corresponds to Al_2O_3. The respective Al2p spectra (Fig. 3d) feature only one peak that is attributed to Al_2O_3. This proves that no AlF_x is formed either during the depth profile measurement or during the polymer deposition step, but instead during the polymer removal or isotropic etch steps.

Since an Al/O ratio higher than of stoichiometric Al_2O_3 therefore indicates the presence of AlF_x, we can use it as a measure of how the fluorination of Al_2O_3 proceeds over the course of several cycles during DRIE. To calculate the amount of fluorinated Al from the Al/O ratio, the following formula was used:

$$\%Al\,fluorinated = 100\% * \left(1 - \frac{\left(\frac{Al}{O}\right)_{min}}{\left(\frac{Al}{O}\right)} \right)$$

Here, $\left(\frac{Al}{O}\right)$ is the measured ratio at the respective sputter time. When reaching the Al_2O_3 in the depth profiling, the measured ratio was always slightly lower than the theoretical value 2/3, most probably because the sensitivity factors slightly deviate from their optimal values. Therefore, it was defined that the lowest measured ratio $\left(\frac{Al}{O}\right)_{min}$ in each profile corresponds to pure Al_2O_3, i.e. 0% fluorination. This approach can lead to an error of a few percent. In particular, in the regions where probably only Al_2O_3 is present, i.e. towards the end of each depth profile, small deviations in the measured ratio Al/O result in the calculation of up to ~5% of fluorinated Al. The results of the calculations are plotted in Fig. 4, and the respective depth profiles are shown in SI Fig. 2. When using t_{pass} = 4.0 s, the maximum degree of fluorination increases from
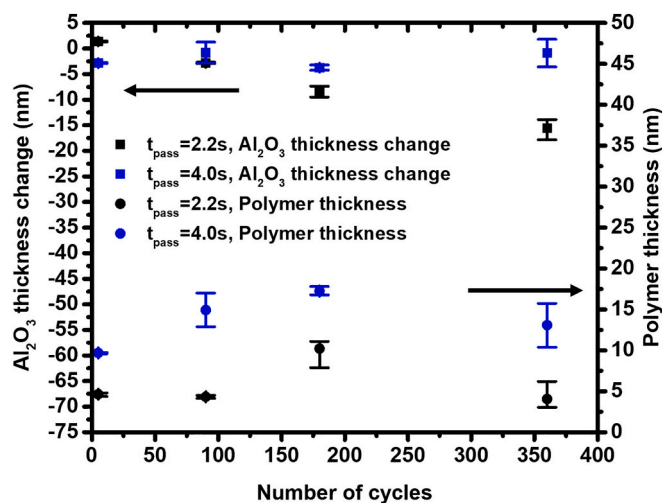

Fig. 2. Plot of the Al_2O_3 thickness change and polymer thickness as a function of the number of DRIE cycles, measured by SE, for two different passivation step times.
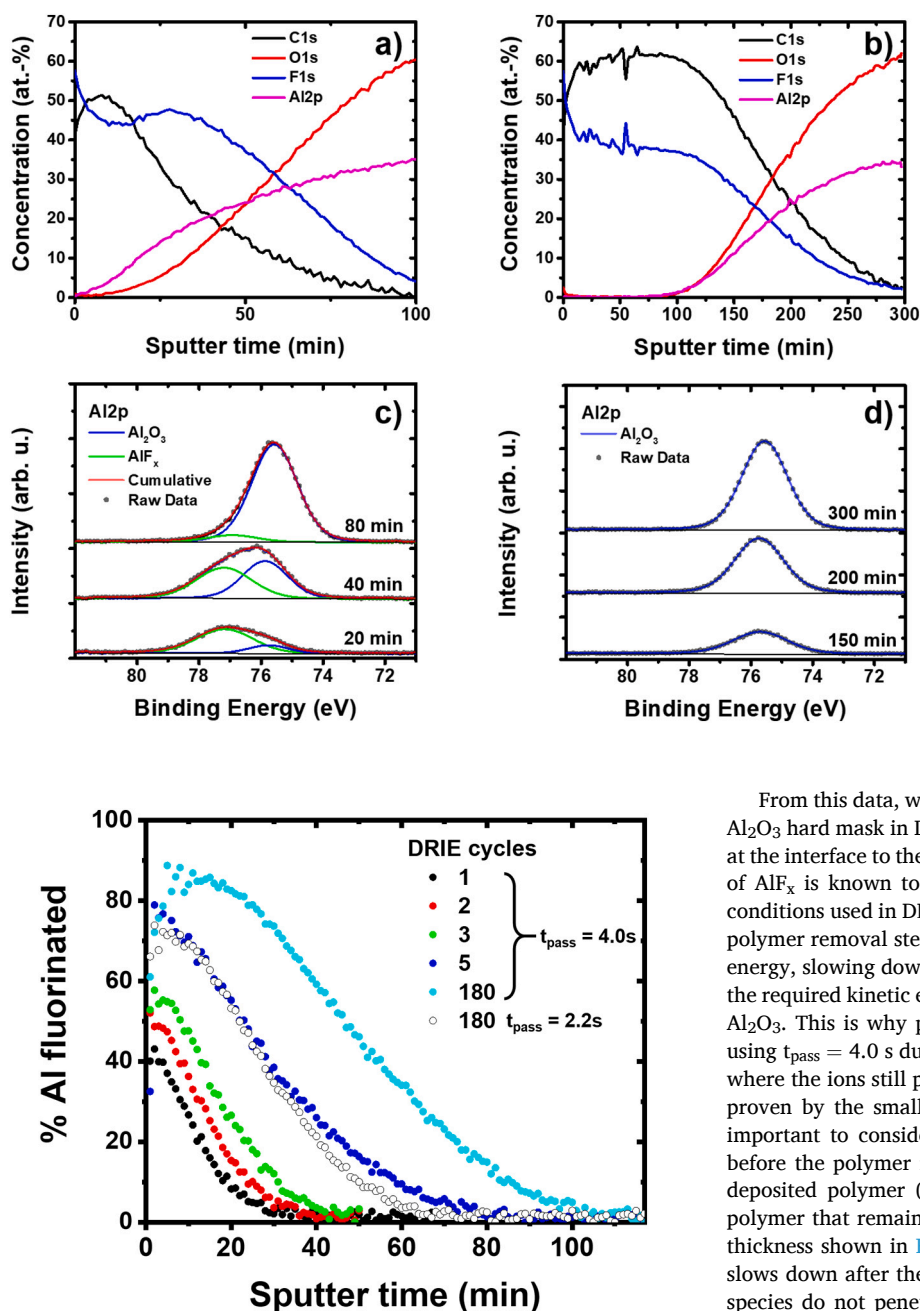
Fig. 3. XPS depth profiles of a) a wafer with 75 nm Al_2O_3 processed for 180 DRIE cycles with t_{pass} = 4.0 s; due to the simultaneous removal of different materials with different sputter rates at the diffuse polymer/Al_2O_3 interface, a reasonable depth information cannot be given, which is why the sputter time is depicted instead; b) a wafer with 75 nm Al_2O_3, on which only the fluorocarbon polymer was deposited using the passivation step 1 in Table 1 with t_{pass} = 4.0 s, resulting in a polymer thickness of ~45 nm; the fluctuations in C and F concentrations at ~60 min sputter time are due to temporary instabilities in the x-ray source; c) Al2p spectra recorded during the depth profile measurement of a), showing the presence of AlF_x; d) Al2p spectra recorded during the depth profile measurement of b), showing only the presence of Al_2O_3, which proves that the AlF_x is formed in the DRIE process and not during depth profiling.

Fig. 4. Plots of the relative amount of fluorinated Al as a function of the sputter time. The investigated samples were processed for various amounts of DRIE cycles using the recipe in Table 1 and t_{pass} = 4.0 s (filled circles), and one was processed for 180 cycles with t_{pass} = 2.2 s (open circles). See the main text for how the calculations were performed.

~40% after one cycle to ~70–80% after five cycles, and then grows slower to ~80–90% after 180 cycles. However when using t_{pass} = 2.2 s, after 180 cycles the maximum degree of fluorination is only ~70%, about as much as after five cycles with t_{pass} = 4.0 s. This data lets us conclude that the amount of AlF_x increases within the first cycles of DRIE relatively fast, and then the rate of formation slows down presumably until a certain thickness is reached. Considering that XPS always probes several nm deep into the surface where the Al/O ratio becomes lower again, it is possible that the real maximum value of fluorination is even higher and that a nearly closed layer of AlF_x is formed in particular with t_{pass} = 4.0 s after 180 cycles. When using a lower passivation time and therefore with a thinner polymer layer on top, less AlF_x is present.

From this data, we can conclude the following etch mechanism of an Al_2O_3 hard mask in DRIE. Already within the first five cycles, the Al_2O_3 at the interface to the polymer becomes fluorinated. Thermal desorption of AlF_x is known to be very slow as it is non-volatile at the process conditions used in DRIE, but it can be removed by sputtering during the polymer removal step. However, the polymer on top attenuates the ion energy, slowing down the sputter removal rate of AlF_x as less ions have the required kinetic energy, and therefore slowing down the etch rate of Al_2O_3. This is why practically no removal of Al_2O_3 is observed when using t_{pass} = 4.0 s due to the thicker polymer, compared to t_{pass} = 2.2 s where the ions still possess sufficient energy to lead to AlF_x desorption, proven by the smaller amount of AlF_x present after 180 cycles. It is important to consider that the total polymer thickness on the Al_2O_3 before the polymer removal step is the sum of the thicknesses of the deposited polymer (e.g. ~45 nm for t_{pass} = 4.0 s, Fig. 3b) and the polymer that remained from the process steps before (the steady-state thickness shown in Fig. 2). With t_{pass} = 4.0 s, the AlF_x formation rate slows down after the first cycles, presumably because the respective F species do not penetrate the already existing AlF_x layer any more to reach the underlying Al_2O_3. Since no AlF_x is removed, the thickness then becomes saturated. The described mechanism is similar to the "chemical sputtering" in continuous etching of SiO_2, Si_3N_4 and Si, where the etch rate drops with increasing steady-state thickness of the polymer film [18]. However, in that case the resulting SiF_4 is volatile and desorbs much more readily even without ion bombardment, resulting in higher etch rate and therefore lower selectivity of a SiO_2 hard mask compared to Al_2O_3, where ion bombardment is necessary to remove the non-volatile AlF_x.

The question remains about the source of the F species responsible for the Al_2O_3 fluorination. It is likely that sputter induced defluorination of the polymer is the source, as this also plays a critical role in continuous etching of $Si/SiO_2/Si_3N_4$ species [17]. Indeed, the C1s signal (Fig. 5a) exhibits the loss of signals attributed to C-F_x towards the interface to Al_2O_3, and only the C-C/C-H signal remains. However, this is also observed for the reference sample of the deposited polymer (Fig. 5b). A defluorination induced by the depth profiling seems unlikely though as the thereby expected formation of AlF_x in the reference sample did not occur, and the C1s signal remains nearly unchanged from
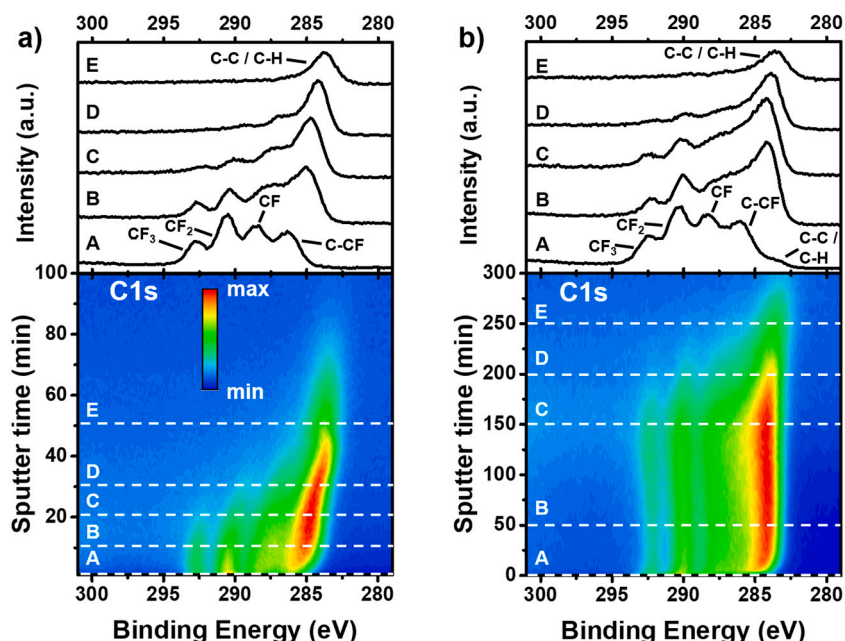
Fig. 5. C1s contour plots a) from the sample presented in Fig. 3a and c, which was processed for 180 DRIE cycles with t_{pass} = 4.0 s; b) from the sample shown in Fig. 3b and d, on which the fluorocarbon polymer was deposited using only the DRIE passivation step for t_{pass} = 4.0 s. The dashed lines mark the spectra that are shown above the contour plot. The presumed bonds responsible for the most intense peaks are depicted. The signals were not deconvoluted due to the probably large number of contributions from different surroundings in the cross-linked polymer. The important observation is that at the interface to the Al_2O_3, the C-F_x contributions vanish and only a C—C / C—H peak remains.

~25–150 min sputter time. Another explanation might be that the polymer contains no F in the initial phase of the deposition, e.g. due to intermixing of carbon with Al_2O_3 and/or exclusive formation of C—C bonds from C_x fragments. A second possible source of F species responsible for the Al_2O_3 fluorination is the SF_6 plasma during the polymer removal and isotropic etch steps. As the polymer removal step had a platen bias applied, it is considered more likely that fluorination would occur in this step due to ion bombardment with F^+ and SF_x^+ species. The fact that no S was detected in depth profiling might be an argument against this. However, it is also possible that the resulting S containing species readily desorb and therefore no S remains implanted in the surface layers. If the F species from the plasma were indeed responsible for the fluorination of Al_2O_3, it would be advantageous to use SF_6 instead of Ar or O_2 as a sputtering gas to maximize the selectivity. Further studies are required to confirm this, and it cannot be ruled out that fluorination occurs due to both, polymer defluorination and reaction with F^+ and SF_x^+ species from the SF_6 plasma.

To put these results into context, we showed that increasing the passivation time leads to an increase in selectivity. As this is caused by reduced AlF_x desorption due to dampening of the ion energy by the polymer layer, a variation of other parameters should in principle lead to similar results. For example, a reduced bias power or higher pressure in the polymer removal step lead to lower average ion energy as well. On the other hand, one also has to consider optimizing the profile of the structure, as well as other aspects such as throughput and possible particle generation, which can all be influenced by the increased passivation time. Therefore, certainly a compromise has to be made between these different aspects, depending on their priority for a particular process. Chamber contamination due to formation of non-volatile AlF_x can be a challenge, particularly in volume manufacturing, which could be alleviated by regular chamber cleaning routines. Compared to a metallic Al mask, it is possible that both Al_2O_3 and Al follow the same principal etch mechanism, as very low etch rates of 0.05 nm/min have been reported for Al in the Bosch process as well [19]. Both materials can exhibit micromasking, which is a challenge that has to be overcome. A systematic comparison of Al_2O_3 and Al regarding the extent of micromasking, and the question whether it can be suppressed in the case of Al_2O_3 like it was shown for Al [5], is subject for further studies.

4. Summary

We investigated the etch mechanism and therefore the origin of the practically infinite selectivity of an Al_2O_3 hard mask in Si DRIE when using a three step Bosch process. SE measurements revealed that the thickness of the fluorocarbon polymer layer on Al_2O_3 increases until an approximate steady-state thickness is reached. An increase in the passivation step time leads to a thicker polymer, as well as a decrease in the Al_2O_3 etch rate, i.e. practically no Al_2O_3 is removed in the example shown after 180 DRIE cycles when using a passivation step time of 4.0 s. XPS depth profiling revealed that during DRIE, AlF_x is formed at the interface between the polymer and the mask. AlF_x is known to be non-volatile, and therefore requires sputtering to be removed. If the polymer layer on top is thick enough to attenuate the incoming ions such that their energy is not sufficient to lead to desorption of AlF_x, the mask does not erode, which is what happens when using a passivation time of 4.0 s. In contrast, when using a passivation time of 2.2 s, the AlF_x can still be removed due to sputtering and the mask selectivity is decreased. This is in contrast to etching of a SiO_2 hard mask, where the resulting SiF_x desorbs even without ion bombardment and therefore the mask erodes faster than Al_2O_3.

Declaration of Competing Interest

The authors declare that they have no known competing financial interests or personal relationships that could have appeared to influence the work reported in this paper.

Appendix A. Supplementary data

Supplementary data to this article can be found online at https://doi.org/10.1016/j.mne.2021.100102.

References

[1] H. Qu, CMOS MEMS Fabrication Technologies and Devices, Micromachines 7 (2016) 1–21, https://doi.org/10.3390/mi7010014.

[2] B. Wu, A. Kumar, S. Pamarthy, High aspect ratio silicon etch: A review, J. Appl. Phys. 108 (2010), https://doi.org/10.1063/1.3474652, pp. 051101/1–20.

[3] P. Ramm, A. Klumpp, J. Weber, M.M. Taaklo, 3D System-on-Chip technologies for More than Moore systems, Microsyst. Technol. 16 (2010) 1051–1055, https://doi.org/10.1007/s00542-009-0976-1.

[4] M. Blauw, G. Craciun, W. Sloof, P. French, E. van der Drift, Advanced time-multiplexed plasma etching of high aspect ratio silicon structures, J. Vac. Sci. Technol. B 20 (2002) 3106–3110, https://doi.org/10.1116/1.1518018.

[5] A. Bagolini, P. Scauso, S. Sanguinetti, P. Bellutti, Silicon Deep Reactive Ion Etching with aluminum hard mask, Mater. Res. Express 6 (2019), https://doi.org/10.1088/2053-1591/ab2423, pp. 085913/1–13.

[6] L.A. Woldering, R.W. Tjerkstra, H.V. Jansen, I.D. Setija, W.L. Vos, Periodic arrays of deep nanopores made in silicon with reactive ion etching and deep UV lithography, Nanotechnology 19 (2008), https://doi.org/10.1088/0957-4484/19/14/145304, pp. 145304/1–11.

[7] M. Henry, S. Walavalkar, A. Homyk, A. Scherer, Alumina etch masks for fabrication of high-aspect-ratio silicon micropillars and nanopillars, Nanotechnology 20 (2009), https://doi.org/10.1088/0957-4484/20/25/255305, pp. 255305/1–4.

[8] J. Dekker, K. Kolari, R. Puurunen, Inductively coupled plasma etching of amorphous Al2O3 and TiO2 mask layers grown by atomic layer deposition, J. Vac. Sci. Technol. B 24 (2006) 2350–2355, https://doi.org/10.1116/1.2353844.

[9] F. Aydinoglu, F. Saffih, R. Dey, B. Cui, Chromium oxide as a hard mask material better than metallic chromium, J. Vac. Sci. Technol. B 35 (2017), https://doi.org/10.1116/1.4998480, pp. 06GB01/1–4.

[10] M. Henry, T. Young, B. Griffin, ScAlN etch mask for highly selective silicon etching, J. Vac. Sci. Technol. B 35 (2017), https://doi.org/10.1116/1.4994841, pp. 052001/1–6.

[11] S. Tegen, P. Moll, Etch Characteristics of Al2O3 in ICP and MERIE Plasma Etchers, J. Electrochem. Soc. 152 (2005), https://doi.org/10.1149/1.1865912.

[12] A. Han, B. Chang, M. Todeschini, H.T. Le, W. Tiddi, M. Keil, Inductively coupled plasma nanoetching of atomic layer deposition alumina, Microelectron. Eng. 193 (2018) 28–33, https://doi.org/10.1016/j.mee.2018.02.023.

[13] K.R. Williams, K. Gupta, M. Wasilik, Etch Rates for Micromachining Processing—Part II, J. Microelectromech. Syst. 12 (2003) 761–778, https://doi.org/10.1109/JMEMS.2003.820936.

[14] J.A. Dean, Lange's Handbook of Chemistry, 15. ed., McGraw-Hill, Inc, 1999.

[15] NIST, X-ray Photoelectron Spectroscopy Database, NIST Standard Reference Database Number 20, National Institute of Standards and Technology, Gaithersburg MD 20899, 2000, https://doi.org/10.18434/T4T88K. Last retrieved October 29th 2021.

[16] P. Sherwood, Introduction to Studies of Aluminum and its Compounds by XPS, Surf. Sci. Spectra 5 (1998) 1–3, https://doi.org/10.1116/1.1247880.

[17] D. Humbird, D. Graves, X. Hua, G. Oehrlein, Molecular dynamics simulations of Ar+-induced transport of fluorine through fluorocarbon films, Appl. Phys. Lett. 84 (2004) 1073–1075, https://doi.org/10.1063/1.1644338.

[18] M. Schaepkens, G. Oehrlein, A review of SiO2 etching studies in inductively coupled fluorocarbon plasmas, J. Electrochem. Soc. 148 (2001) C211–C221, https://doi.org/10.1149/1.1348260.

[19] A. Bagolini, S. Ronchin, P. Bellutti, M. Chistè, M. Verotti, N.P. Belfiore, Fabrication of Novel MEMS Microgrippers by Deep Reactive Ion Etching With Metal Hard Mask, J. Microelectromech. Syst. 26 (2017) 926–934, https://doi.org/10.1109/JMEMS.2017.2696033.